Supporting Information

Cation Control of Cooperative CO_2 Adsorption in Li-containing Mixed Cation forms of the Flexible Zeolite Merlinoite

Veselina M. Georgieva,[1,†] Elliott L. Bruce,[1,†] Ruxandra G. Chitac,[1] Magdalena M. Lozinska,[1] Anna M. Hall,[1] Claire A. Murray,[2] Ronald I. Smith,[3] Alessandro Turrina[4] and Paul A. Wright[1,*]

[1] EaStCHEM School of Chemistry, University of St Andrews, Purdie Building, North Haugh, St Andrews, KY16 9ST, UK. Email: paw2@st-andrews.ac.uk

[2] Diamond Light Source, Harwell Science and Innovation Campus, Didcot, OX11 0DE, UK

[3] ISIS Neutron and Muon Source, Rutherford Appleton Laboratory, Harwell Campus, Didcot, OX11 0QX, UK

[4] Johnson Matthey Technology Centre, Chilton P.O. Box 1, Belasis Avenue, Billingham TS23 1LB, UK

† These authors contributed equally

1. Analytical details for Li-containing MER zeolites Li-MER and Li,Na-MER

Weighed amounts (~0.08-0.12 g) of $Li_{6.2}$-MER or $Li_{6.2-x}Na_x$-MER zeolites were stirred with 10.0 mL of 1 M ammonium chloride solution in 60 ml beakers held at 333 K for 30 mins. The ion exchange was repeated three successive times on each zeolite and the solutions from all three ion exchanges were filtered into the same 50.0 ml volumetric flasks. Deionised water was added to complete filling to the calibration mark. A final, fourth, ion exchange was collected separately into 50.0 ml volumetric flasks to confirm that three ion exchanges were sufficient to remove all the Li^+ cations. The expected amount of Li^+ ions lost to the solution during ion exchanges was calculated. In order to quantitatively determine Li^+ cations in the zeolite MER the inductively coupled plasma - optical emission spectrometry (ICP-OES) was used. The calibration curves were provided and were selected according to the expected concentrations of Li^+ cations in the sample solutions. Standard solutions were prepared by diluting the standard Li solution (TraceCERT®, 1000 mg/L Li in nitric acid) with water and a blank sample contained ammonium chloride solution and deionised water used for ion exchange. The analytical characteristic of the ion exchange of Li-MER samples, including concentration of Li in the solution and number of cations per unit cell is summarised in Table 2.1.

Table S1. The analytical characteristic of the ion exchange of $Li_{6.2}$-MER and $Li_{6.2-x}Na_x$-MER.

Sample	Expected concentration of Li in the solution after three ion exchanges (ppm)	Measured concentration of Li in the solution after three ion exchanges (ppm)	Measured concentration of Li in the solution after fourth ion exchange (ppm)	Cations in the solution (lower limit)/ unit cell
$Li_{6.2}$-MER	0.8364	0.7847	0.0091	5.9
$Li_{5.2}Na_{1.0}$-MER	0.6957	0.6317	0.0047	4.7
$Li_{4.2}Na_{2.0}$-MER	0.4332	0.3879	0.0029	3.8
$Li_{3.0}Na_{3.2}$-MER	0.4237	0.3957	0.0022	2.8
$Li_{1.9}Na_{4.3}$-MER	0.1883	0.1678	0.0009	1.7
$Li_{0.9}Na_{5.3}$-MER	0.1318	0.1889	0.0009	1.3

2. Crystallography

2.1 PXRD patterns of MER materials

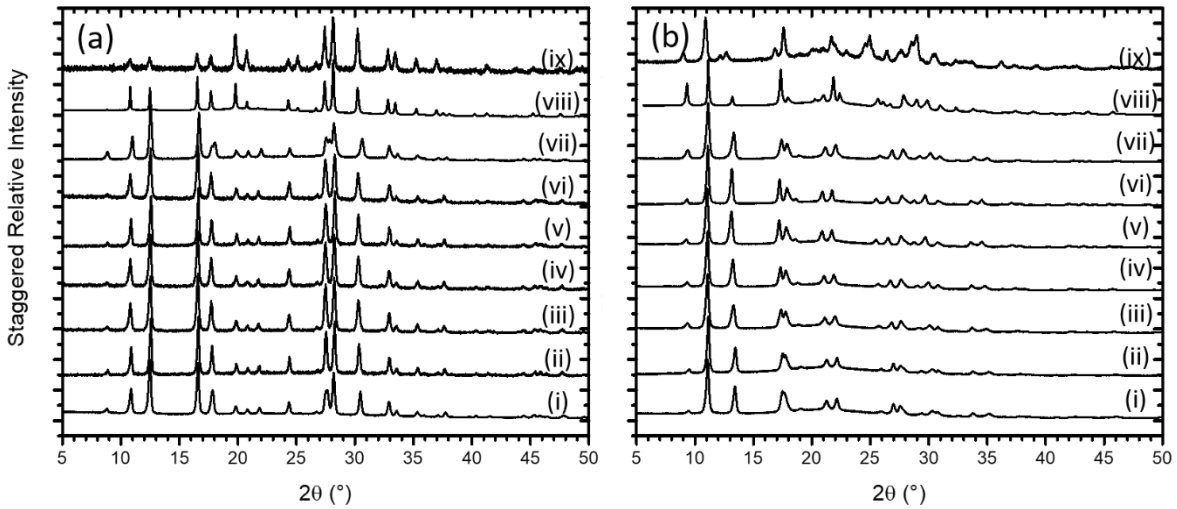

Figure S1. Scaled PXRD patterns of (a) hydrated and (b) dehydrated MER samples: (i) $Li_{6.2}$-, (ii) $Li_{5.0}Na_{1.2}$-, (iii) $Li_{4.0}Na_{2.2}$-, (iv) $Li_{3.0}Na_{3.2}$-, (v) $Li_{2.0}Na_{4.2}$-, (vi) $Li_{1.0}Na_{5.2}$, (vii) $Li_{4.0}K_{2.2}$-, (viii) $Li_{3.4}Cs_{2.8}$- and (ix) $Li_{1.0}Cs_{5.2}$-MER.

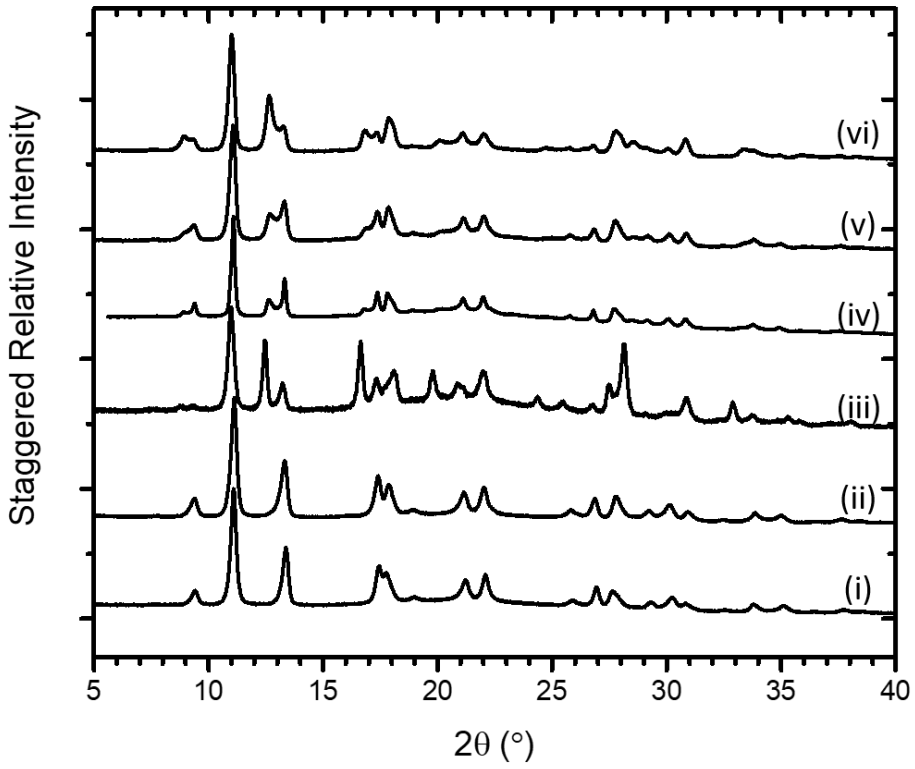

Figure S2. Scaled PXRD patterns of dehydrated Li,K-MER samples: (i) $Li_{5.0}K_{1.2}$-, (ii) $Li_{4.0}K_{2.2}$-, (iii) $Li_{3.7}K_{2.5}$-, (iv) $Li_{3.0}K_{3.2}$-, (v) $Li_{2.0}K_{4.2}$- and (vi) $Li_{1.0}K_{5.2}$-MER.

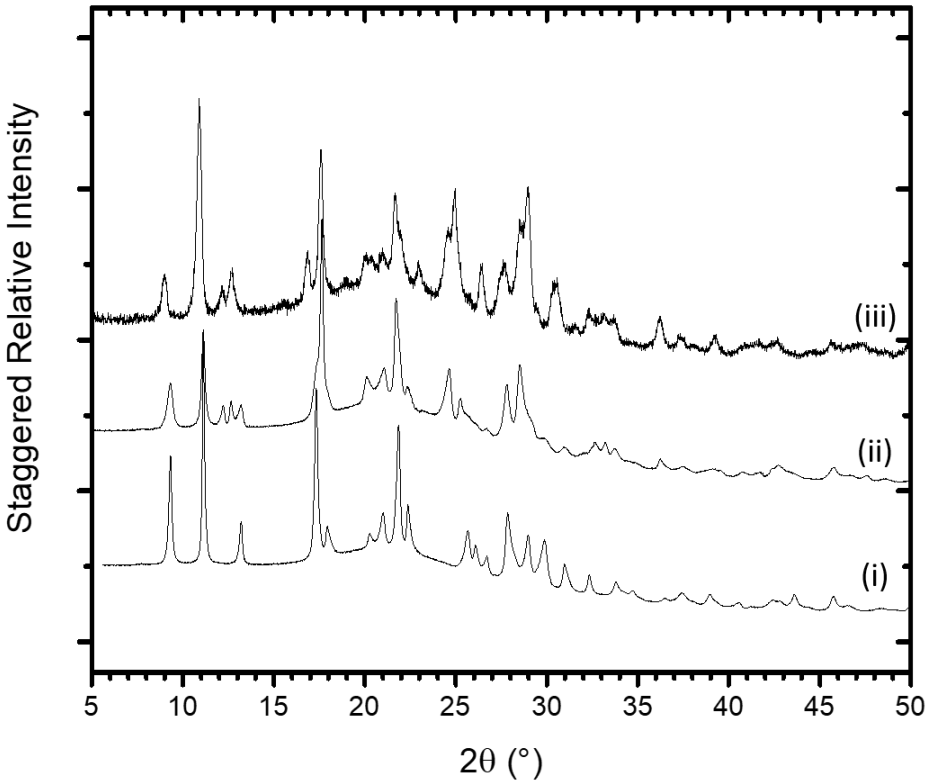

Figure S3. Scaled PXRD patterns of dehydrated Li,Cs-MER samples: (i) $Li_{3.4}Cs_{2.8}$-, (ii) $Li_{3.0}Cs_{3.2}$- and (iii) $Li_{1.0}Cs_{5.2}$-MER.

2.1 Refinement Summary

Table S2. PXRD Refinement details of all single-phase MER materials investigated.

Sample	$Li_{6.2}$-MER (dh)	$Li_{6.2}$-MER (h)	$Li_{5.0}Na_{1.2}$-MER (dh)	$Li_{4.0}Na_{2.2}$-MER (dh)	$Li_{3.0}Na_{3.2}$-MER (dh)
Unit Cell	$[Si_{25.9}Al_{6.1}O_{64}].O_{1.0}$	$[Si_{25.9}Al_{6.1}O_{64}].O_{18.2}$	$[Si_{25.9}Al_{6.1}O_{64}]$	$Na_{1.9}[Si_{25.9}Al_{6.1}O_{64}]$	$Na_{2.6}[Si_{25.9}Al_{6.1}O_{64}]$
***T* (K)**	298	298	298	298	298
Space Group	*Immm*	*Immm*	*Immm*	*Immm*	*Immm*
X-ray Source	Stoe	Stoe	Stoe	Stoe	Stoe
l (Å)	1.54056	1.54056	1.54056	1.54056	1.54056
***a* (Å)**	13.206(1)	14.150(1)	13.240(1)	13.297(1)	13.339(1)
***b* (Å)**	13.141(1)	14.145(1)	13.172(1)	13.263(1)	13.343(1)
***c* (Å)**	9.976(1)	9.926(1)	9.985(1)	9.946(1)	9.948(1)
***V* (Å^3)**	1731.2(2)	1986.6(2)	1741.3(3)	1754.1(2)	1770.6(2)
R_p	2.6%	4.7%	3.5%	3.1%	3.2%
R_{wp}	3.5%	6.4%	4.6%	4.1%	4.1%
χ^2	1.8	1.9	1.7	1.7	1.6

Sample	$Li_{5.0}K_{1.2}$-MER (dh)	$Li_{4.0}K_{2.2}$-MER (dh)	$Li_{3.4}Cs_{2.8}$-MER (dh)	$Li_{3.4}Cs_{2.8}$-MER (h)	$Li_{3.4}Cs_{2.8}$-MER (ads)
Unit Cell	$K_{0.7}[Si_{25.9}Al_{6.1}O_{64}]$	$K_{1.7}[Si_{25.9}Al_{6.1}O_{64}]$	$Cs_{2.4}[Si_{25.9}Al_{6.1}O_{64}]$	$Cs_{3.1}[Si_{25.9}Al_{6.1}O_{64}].O_{15.2}$	$Cs_{2.9}[Si_{25.9}Al_{6.1}O_{64}].(CO_2)_{8.3}$
***T* (K)**	298	298	298	298	298
Space Group	*Immm*	*Immm*	*Immm*	*Immm*	*Immm*
X-ray Source	Stoe	I11, DLS	I11, DLS	I11, DLS	I11, DLS
l (Å)	1.54056	0.826398	0.826398	0.826398	0.826398
***a* (Å)**	13.225(1)	13.275(1)	13.337(1)	14.153(1)	14.088(1)
***b* (Å)**	13.179(1)	13.244(1)	13.377(1)	14.154(1)	14.099(1)
***c* (Å)**	9.938(1)	9.907(1)	9.837(1)	10.003(1)	10.028(1)
***V* (Å^3)**	1732.2(2)	1741.7(2)	1755.0(2)	2003.8(2)	1991.8(2)
R_p	3.4%	2.0%	2.0%	3.0%	2.4%
R_{wp}	4.5%	2.9%	3.0%	4.7%	3.3%
χ^2	1.8	2.1	2.3	2.5	1.9

Table S3. Refinement details of $Li_{3.7}K_{2.5}$-MER (dh) and its low and high K phases.

Sample	**$Li_{3.7}K_{2.5}$-MER (dh)**	
***T* (K)**	298	
X-ray Source	I11, DLS	
l (Å)	0.826398	
Phase	Low K	High K
Unit Cell	$K_{2.6}[Si_{25.9}Al_{6.1}O_{64}].O_x$	$K_{6.9}[Si_{25.9}Al_{6.1}O_{64}].O_x$
Space Group	*Immm*	*Immm*
***a* (Å)**	13.353(1)	14.144(1)
***b* (Å)**	13.271(1)	14.145(1)
***c* (Å)**	9.898(1)	9.764(1)
***V* (Å^3)**	1753.9(3)	1953.3(3)
R_p	2.2%	
R_{wp}	3.2%	
χ^2	2.1	

2.1 Crystallographic Information

Table S4. $Li_{6.2}$-MER (h)

Site	Type	x	y	z	Occ.	Ω	B_{iso}
Ow1	O	0	0	0.719(1)	1.00	4	2
Ow2	O	0.5	0.5	0.5	1.00	2	2
Ow3	O	0.313(1)	0.439(1)	0.000(1)	0.50(1)	16	2
Ow4	O	0.452(2)	0.402(2)	0	0.53(2)	8	2
O1	O	0.168(2)	0.159(1)	0.202(1)	1	16	1
O2	O	0.115(2)	0.278(2)	0	1	8	1
O5	O	0.696(1)	0.129(2)	0	1	8	1
O3	O	0	0.226(1)	0.196(3)	1	8	1
O6	O	0.752(2)	0	0.187(3)	1	8	1
O4	O	0.142(1)	0.350(1)	0.248(3)	1	16	1
Si1	Si	0.106(1)	0.254(1)	0.158(1)	0.81	16	1
Al1	Al	0.106(1)	0.254(1)	0.158(1)	0.19	16	1
Si2	Si	0.731(1)	0.109(1)	0.157(1)	0.81	16	1
Al2	Al	0.731(1)	0.109(1)	0.157(1)	0.19	16	1

Table S5. $Li_{6.2}$-MER (dh)

Site	Type	x	y	z	Occ.	Ω	B_{iso}
O1	O	0.200(1)	0.122(1)	0.184(1)	1	16	1
O2	O	0.120(1)	0.244(1)	0	1	8	1
O5	O	0.647(1)	0.131(1)	0	1	8	1
O3	O	0	0.154(1)	0.181(2)	1	8	1
O6	O	0.644(1)	0	0.214(2)	1	8	1
O4	O	0.124(1)	0.301(1)	0.251(1)	1	16	1
Si1	Si	0.112(1)	0.206(1)	0.153(1)	0.81	16	1
Al1	Al	0.112(1)	0.206(1)	0.153(1)	0.19	16	1
Si2	Si	0.678(1)	0.114(1)	0.160(1)	0.81	16	1
Al2	Al	0.678(1)	0.114(1)	0.160(1)	0.19	16	1
Ow1	O	0.5	0.5	0	0.52(2)	2	2

Table S6. $Li_{5.0}Na_{1.2}$-MER (dh)

Site	Type	x	y	z	Occ.	Ω	B_{iso}
O1	O	0.202(1)	0.123(1)	0.180(1)	1	16	1
O2	O	0.115(1)	0.245(1)	0	1	8	1
O5	O	0.650(2)	0.127(1)	0	1	8	1
O3	O	0	0.154(1)	0.178(2)	1	8	1
O6	O	0.643(1)	0	0.216(3)	1	8	1
O4	O	0.127(1)	0.302(1)	0.253(2)	1	16	1
Si1	Si	0.114(1)	0.207(1)	0.151(1)	0.81	16	1
Al1	Al	0.114(1)	0.207(1)	0.151(1)	0.19	16	1
Si2	Si	0.679(1)	0.113(1)	0.159(1)	0.81	16	1
Al2	Al	0.679(1)	0.113(1)	0.159(1)	0.19	16	1

Table S7. $Li_{4.0}Na_{2.2}$-MER (dh)

Site	Type	x	y	z	Occ.	Ω	B_{iso}
O1	O	0.198(1)	0.127(1)	0.182(1)	1	16	1
O2	O	0.121(1)	0.251(1)	0	1	8	1
O5	O	0.654(1)	0.127(1)	0	1	8	1
O3	O	0	0.161(1)	0.178(2)	1	8	1
O6	O	0.650(1)	0	0.208(2)	1	8	1
O4	O	0.124(1)	0.306(1)	0.254(1)	1	16	1
Si1	Si	0.110(1)	0.210(1)	0.154(1)	0.81	16	1
Al1	Al	0.110(1)	0.210(1)	0.154(1)	0.19	16	1
Si2	Si	0.683(1)	0.113(1)	0.158(1)	0.81	16	1
Al2	Al	0.683(1)	0.113(1)	0.158(1)	0.19	16	1
Na1	Na	0	0	0.767(1)	0.14(2)	4	2
Na2	Na	0	0.5	0.885(1)	0.34(2)	4	2

Table S8. $Li_{3.0}Na_{3.2}$-MER (dh)

Site	Type	x	y	z	Occ.	Ω	B_{iso}
O1	O	0.196(1)	0.128(1)	0.180(1)	1	16	1
O2	O	0.118(1)	0.253(1)	0	1	8	1
O5	O	0.654(1)	0.126(1)	0	1	8	1
O3	O	0	0.161(1)	0.179(1)	1	8	1
O6	O	0.652(1)	0	0.212(1)	1	8	1
O4	O	0.123(1)	0.307(1)	0.252(1)	1	16	1
Si1	Si	0.110(1)	0.213(1)	0.154(1)	0.81	16	1
Al1	Al	0.110(1)	0.213(1)	0.154(1)	0.19	16	1
Si2	Si	0.683(1)	0.114(1)	0.158(1)	0.81	16	1
Al2	Al	0.683(1)	0.114(1)	0.158(1)	0.19	16	1
Na1	Na	0	0	0.760(1)	0.29(2)	4	2
Na2	Na	0.5	0.213(1)	0	0.14(2)	4	2
Na3	Na	0	0.5	0.875(1)	0.23(2)	4	2

Table S9. $Li_{5.0}K_{1.2}$-MER (dh)

Site	Type	x	y	z	Occ.	Ω	B_{iso}
O1	O	0.203(1)	0.123(1)	0.179(1)	1	16	1
O2	O	0.122(1)	0.249(1)	0	1	8	1
O5	O	0.649(1)	0.128(1)	0	1	8	1
O3	O	0	0.151(1)	0.171(2)	1	8	1
O6	O	0.650(1)	0	0.223(2)	1	8	1
O4	O	0.123(1)	0.301(1)	0.257(1)	1	16	1
Si1	Si	0.112(1)	0.211(1)	0.146(1)	0.81	16	1
Al1	Al	0.112(1)	0.211(1)	0.146(1)	0.19	16	1
Si2	Si	0.676(1)	0.113(1)	0.162(1)	0.81	16	1
Al2	Al	0.676(1)	0.113(1)	0.162(1)	0.19	16	1
K1	K	0	0.5	0.076(1)	0.17(1)	4	2

Table S10. $Li_{4.0}K_{2.2}$-MER (dh)

Site	Type	x	y	z	Occ.	Ω	B_{iso}
O1	O	0.200(1)	0.122(1)	0.172(1)	1	16	1
O2	O	0.123(1)	0.245(1)	0	1	8	1
O5	O	0.649(1)	0.133(1)	0	1	8	1
O3	O	0	0.158(1)	0.177(2)	1	8	1
O6	O	0.650(1)	0.000	0.207(2)	1	8	1
O4	O	0.125(1)	0.301(1)	0.257(1)	1	16	1
Si1	Si	0.113(1)	0.209(1)	0.149(1)	0.81	16	1
Al1	Al	0.113(1)	0.209(1)	0.149(1)	0.19	16	1
Si2	Si	0.678(1)	0.112(1)	0.162(1)	0.81	16	1
Al2	Al	0.678(1)	0.112(1)	0.162(1)	0.19	16	1
K1	K	0	0.154(1)	0.5	0.11(1)	4	2
K2	K	0	0.5	0.086(1)	0.33(1)	4	2

Table S11. $Li_{3.4}Cs_{2.8}$-MER (dh)

Site	Type	x	y	z	Occ.	Ω	B_{iso}
O1	O	0.196(1)	0.128(1)	0.169(1)	1	16	1
O2	O	0.117(1)	0.249(1)	0	1	8	1
O5	O	0.645(1)	0.117(1)	0	1	8	1
O3	O	0	0.159(1)	0.203(1)	1	8	1
O6	O	0.660(1)	0	0.206(2)	1	8	1
O4	O	0.128(1)	0.304(1)	0.254(1)	1	16	1
Si1	Si	0.109(1)	0.207(1)	0.151(1)	1	16	1
Al1	Al	0.109(1)	0.207(1)	0.151(1)	1	16	1
Si2	Si	0.681(1)	0.116(1)	0.154(1)	1	16	1
Al2	Al	0.681(1)	0.116(1)	0.154(1)	1	16	1
Cs2	Cs	0	0.5	0	0.91(1)	2	2
Cs1	Cs	0.446(1)	0.5	0.082(2)	0.08(1)	8	2

Table S12. $Li_{3.4}Cs_{2.8}$-MER (h)

Site	Type	x	y	z	Occ.	Ω	B_{iso}
Cs1	Cs	0	0	0.247(1)	0.35(1)	4	2
Cs2	Cs	0	0.5	0	0.30(1)	2	2
Cs3	Cs	0.5	0.181(1)	0	0.28(1)	4	2
Ow1	O	0	0	0.663(1)	1	4	2
Ow2	O	0.5	0.5	0.5	1	2	2
Ow3	O	0.296(1)	0.385(1)	0.026(1)	0.24(1)	16	2
Ow4	O	0.420(1)	0.358(1)	0	0.67(1)	8	2
O1	O	0.168(1)	0.156(1)	0.199(1)	1	16	1
O2	O	0.124(1)	0.306(1)	0	1	8	1
O5	O	0.703(1)	0.113(1)	0	1	8	1
O3	O	0	0.232(1)	0.171(2)	1	8	1
O6	O	0.745(1)	0	0.207(1)	1	8	1
O4	O	0.140(1)	0.344(1)	0.258(2)	1	16	1
Si1	Si	0.108(1)	0.261(1)	0.165(1)	0.81	16	1
Al1	Al	0.108(1)	0.261(1)	0.165(1)	0.19	16	1
Si2	Si	0.733(1)	0.110(1)	0.156(1)	0.81	16	1
Al2	Al	0.733(1)	0.110(1)	0.156(1)	0.19	16	1

Table S13. $Li_{3.4}Cs_{2.8}$-MER (ads)

Site	Type	x	y	z	Occ.	Ω	B_{iso}
Cs1	Cs	0	0	0.245(1)	1	4	2
Cs2	Cs	0	0.5	0	1	2	2
Cs3	Cs	0.5	0.232(1)	0	1	4	2
O1	O	0.160(1)	0.170(1)	0.188(1)	1	16	1
O2	O	0.124(1)	0.307(1)	0	1	8	1
O5	O	0.714(1)	0.119(1)	0	1	8	1
O3	O	0	0.256(2)	0.210(1)	1.00	8	1
O6	O	0.770(1)	0	0.197(1)	1.00	8	1
O4	O	0.160(1)	0.359(1)	0.237(1)	1.00	16	1
Si1	Si	0.111(1)	0.269(1)	0.160(1)	0.81	16	1
Al1	Al	0.111(1)	0.269(1)	0.160(1)	0.19	16	1
Si2	Si	0.742(1)	0.108(1)	0.161(1)	0.81	16	1
Al2	Al	0.742(1)	0.108(1)	0.161(1)	0.19	16	1
C1	C	0.5	0.5	0	0.61(1)	2	2
OC1	O	0.5	0.5	0.116	0.61(1)	4	2
C2	C	0.172(1)	0	0.5	0.91(1)	4	2
OC2	O	0.172(1)	0.918	0.5	0.91(1)	8	2
C3	C	0	0.5	0.5	1.00(2)	2	2
OC3	O	0	0.5	0.616	1.00(2)	4	2
C4	C	0	0.5	0	0.81(1)	2	2
OC4	O	0	0	0.116	0.81(1)	4	2

$Li_{3.7}K_{2.5}$-MER Phases

Table S14. $Li_{3.7}K_{2.5}$-MER (dh – Low K phase)

Site	Type	x	y	z	Occ.	Ω	B_{iso}
O1	O	0.189(2)	0.117(2)	0.203(2)	1	16	1
O2	O	0.141(2)	0.232(3)	0	1	8	1
O5	O	0.684(3)	0.138(3)	0	1	8	1
O3	O	0	0.172(2)	0.168(4)	1	8	1
O6	O	0.651(2)	0	0.189(5)	1	8	1
O4	O	0.133(2)	0.305(2)	0.25(3)	1	16	1
Si1	Si	0.114(1)	0.205(1)	0.154(2)	0.81	16	1
Si1	Al	0.114(1)	0.205(1)	0.154(2)	0.19	16	1
Si2	Si	0.693(1)	0.113(1)	0.160(2)	0.81	16	1
Si2	Al	0.693(1)	0.113(1)	0.160(2)	0.19	16	1
K1	K	0.059(3)	0.5	0	0.50(2)	4	2
K2	K	0	0.648(1)	0.5	0.16(3)	4	2
Ow1	O	0.5	0.5	0	1	2	2

Table S15. $Li_{3.7}K_{2.5}$-MER (dh – High K phase)

Site	Type	x	y	z	Occ.	Ω	B_{iso}
O1	O	0.169(2)	0.166(2)	0.189(1)	1	16	1
O2	O	0.111(2)	0.284(2)	0	1	8	1
O5	O	0.706(2)	0.124(2)	0	1	8	1
O3	O	0	0.240(2)	0.205(4)	1	8	1
O6	O	0.751(2)	0	0.187(4)	1	8	1
O4	O	0.149(2)	0.349(2)	0.247(4)	1	16	1
Si1	Si	0.103(1)	0.259(1)	0.166(1)	0.81	16	1
Al1	Al	0.103(1)	0.259(1)	0.166(1)	0.19	16	1
Si2	Si	0.734(1)	0.109(1)	0.156(1)	0.81	16	1
Al2	Al	0.734(1)	0.109(1)	0.156(1)	0.19	16	1
K1	K	0	0	0.230(1)	0.69(1)	4	2
K2	K	0.156(1)	0.5	0	0.83(1)	4	2
K3	K	0	0.534(4)	0.5	0.22(1)	4	2
Ow1	O	0.5	0.5	0	1	2	2

2.1 Rietveld Plots

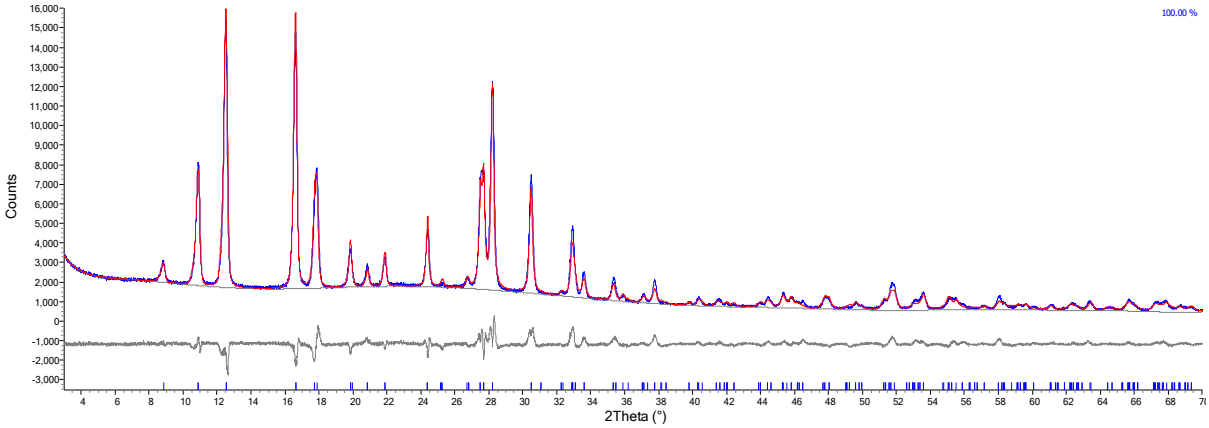

Figure S4. $Li_{6.2}$-MER (h) Rietveld plot

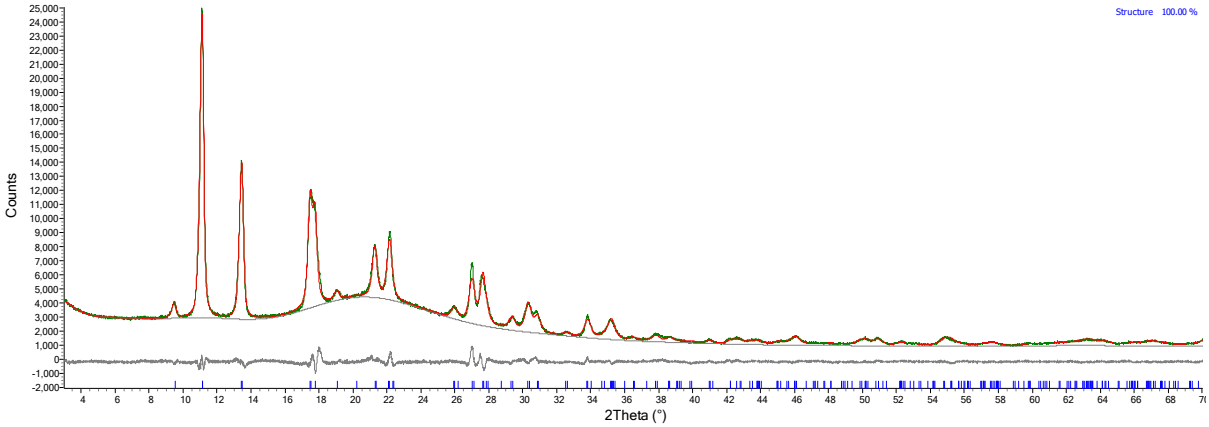

Figure S5. $Li_{6.2}$-MER (dh) Rietveld plot

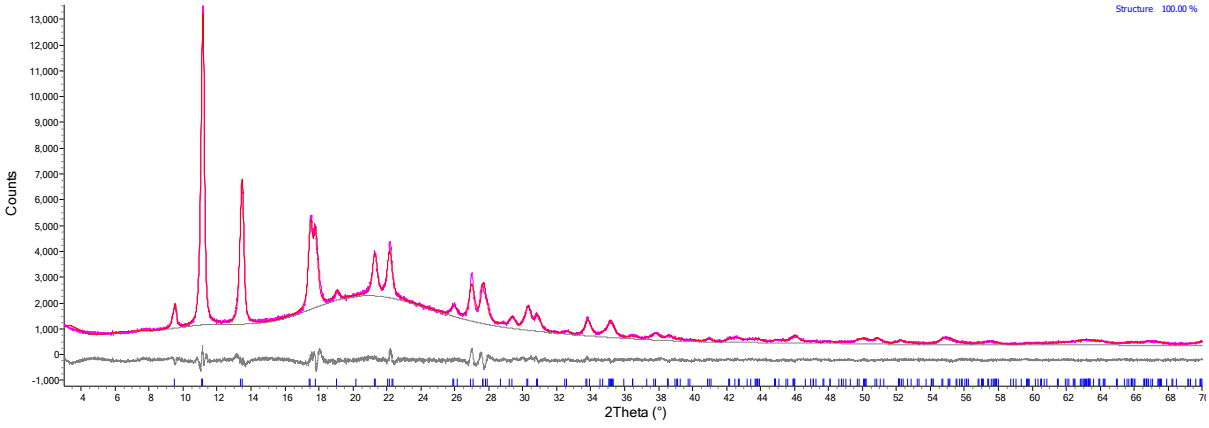

Figure S6. $Li_{5.0}Na_{1.2}$-MER (dh) Rietveld plot

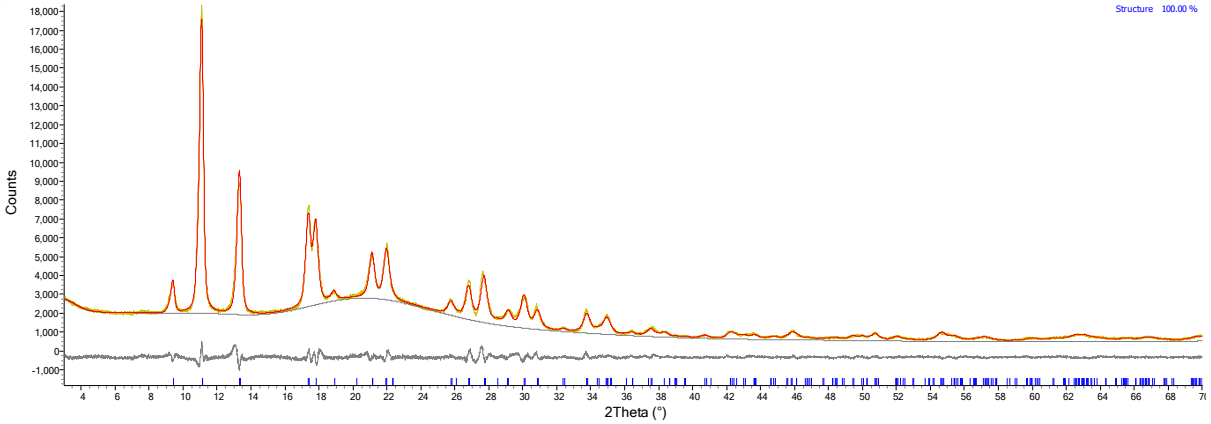

Figure S7. $Li_{4.0}Na_{2.2}$-MER (dh) Rietveld plot

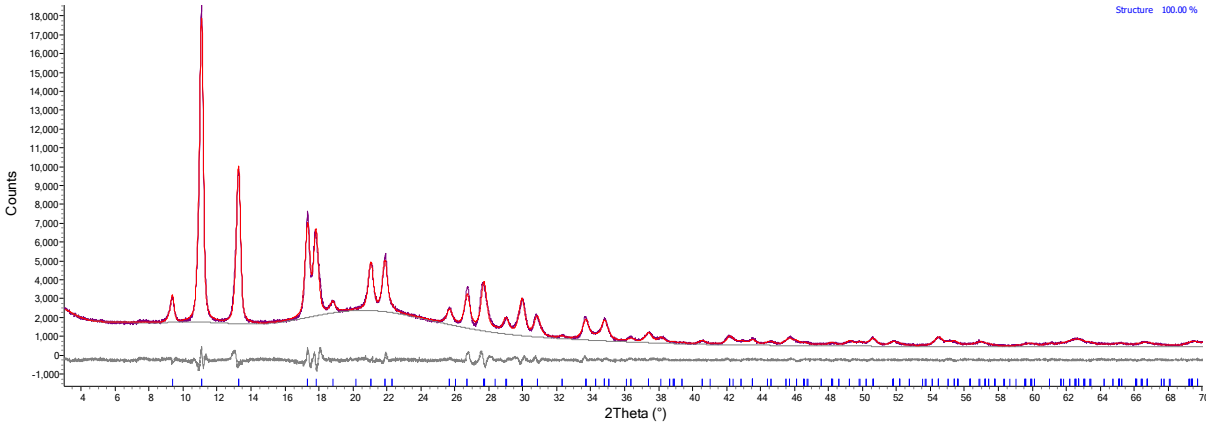

Figure S8. $Li_{3.0}Na_{3.3}$-MER (dh) Rietveld plot

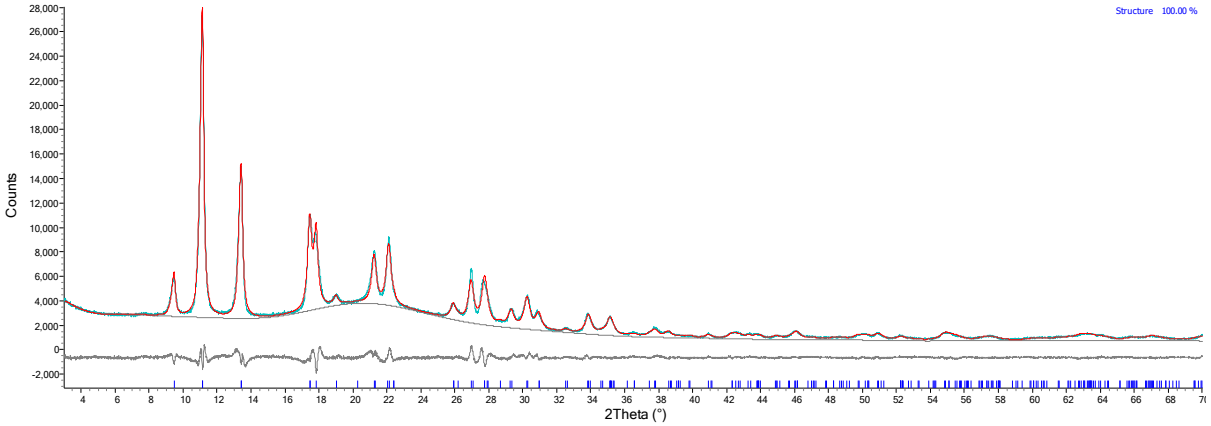

Figure S9. $Li_{5.0}K_{1.2}$-MER (dh) Rietveld plot

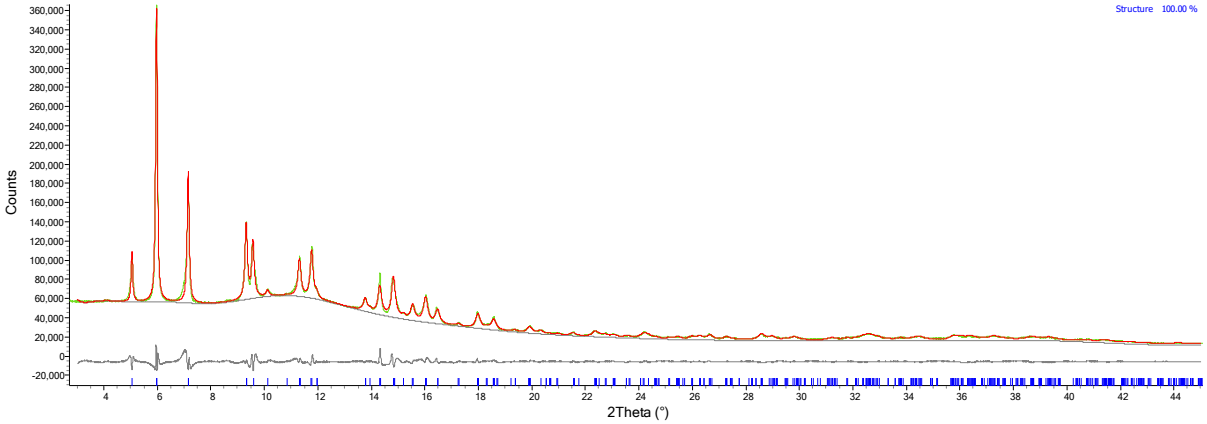

Figure S10. $Li_{4.0}K_{2.2}$-MER (dh) Rietveld plot

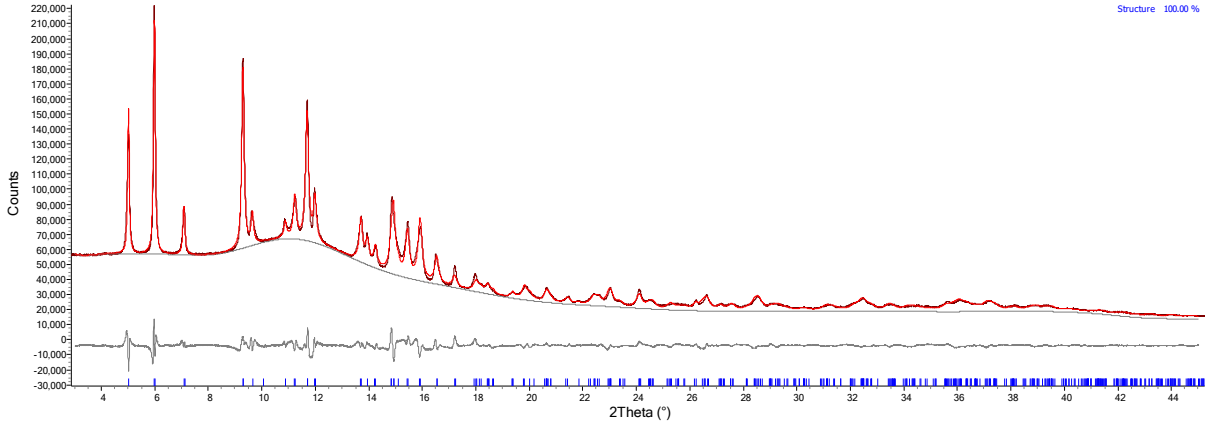

Figure S11. $Li_{4.0}K_{2.2}$-MER (h) Rietveld plot

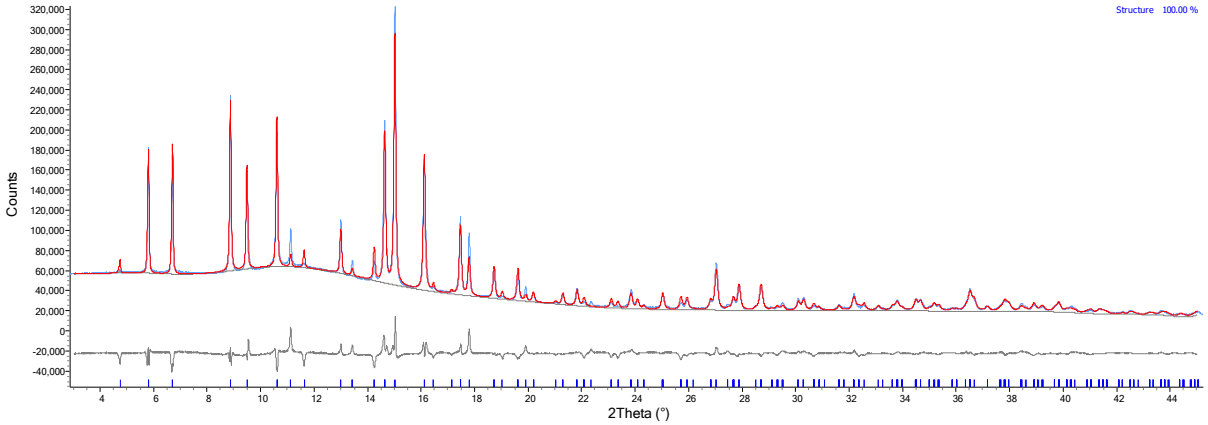

Figure S12. $Li_{3.4}Cs_{2.8}$-MER (h) Rietveld plot

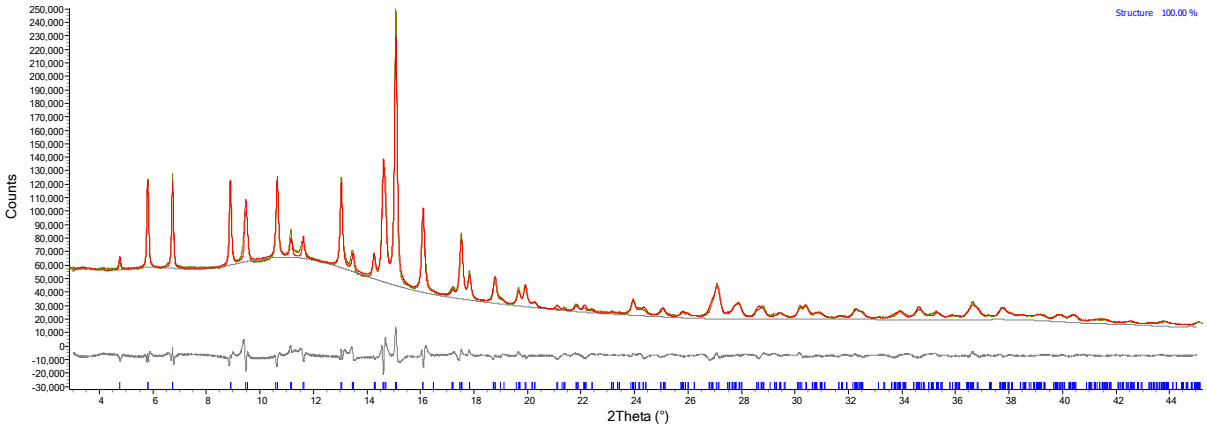

Figure S13. $Li_{3.4}Cs_{2.8}$-MER (ads) Rietveld plot

$Li_{3.7}K_{2.5}$-MER showing exsolution when dehydrated

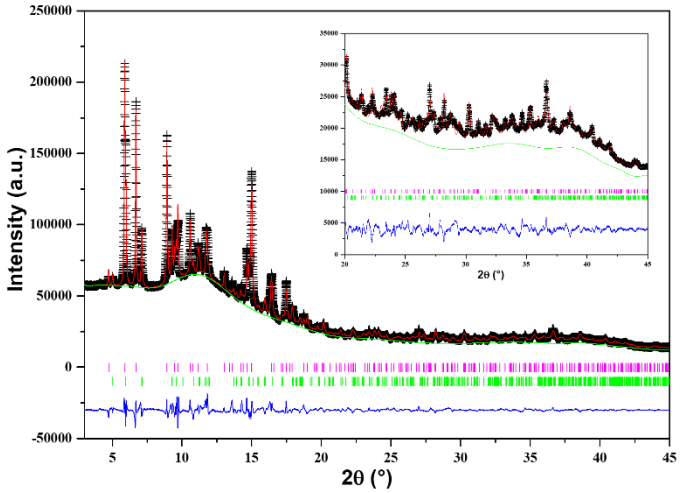

Figure S14. Rietveld plot of dehydrated $Li_{3.7}K_{2.5}$-MER, with expansion of higher angle data shown inset. The fit includes 2 phases, a K-rich and a K-poor phase.

2.2 Powder Neutron Diffraction of $Li_{6.2}$-MER

Time-of-flight neutron powder diffraction data were recorded on the Polaris diffractometer, ISIS, at 298 K.

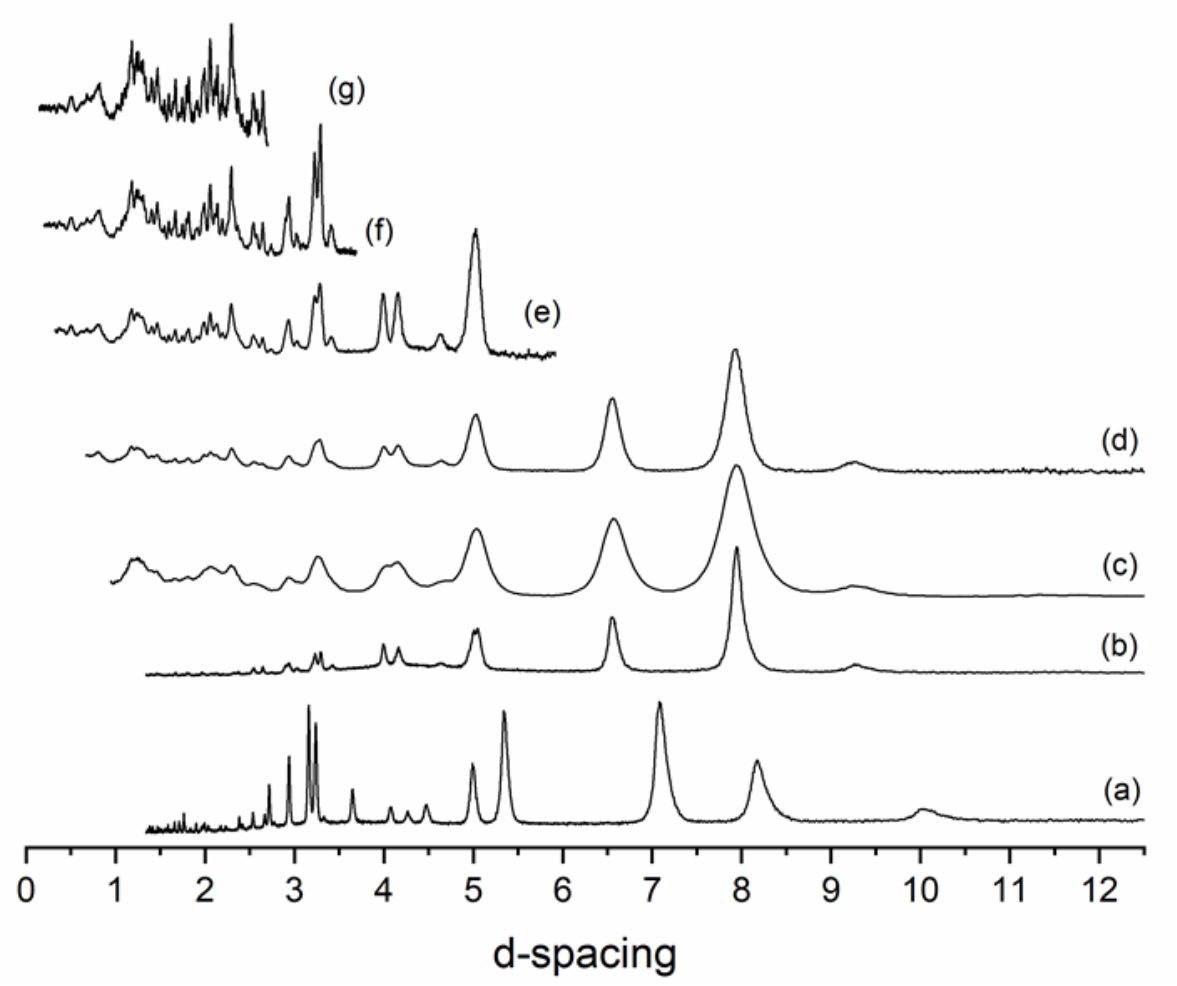

Figure S15. Comparison of (a) hydrated and (b) dehydrated $Li_{6.2}$-MER laboratory PXRD data with neutron diffraction data for dehydrated $Li_{6.2}$-MER sample, (c) bank 1, (d) bank 2, (e) bank 3, (f) bank 4 and (g) bank 5.

(a)

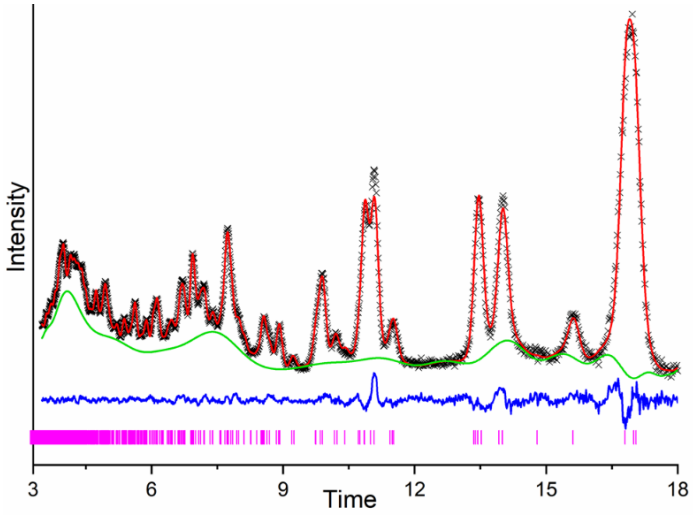

(b)

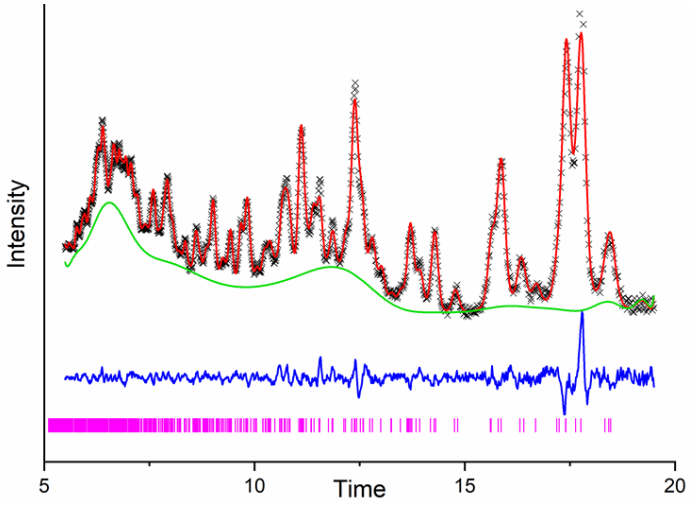

(c)

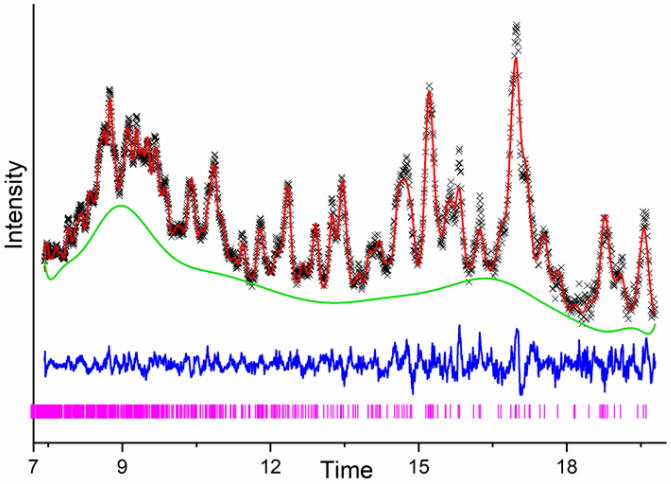

Figure S16. Rietveld plots of neutron diffraction profiles (T = 298 K) of dehydrated $Li_{6.2}$-MER zeolite, (a) bank 3, (b) bank 4 and (c) bank 5 (Observed – black, calculated – red, difference – blue, reflection position markers – pink and background – green).

Table S16. Crystallographic details of dehydrated $Li_{6.2}$-MER sample

	$Li_{6.2}$-MER
Unit cell	$Li_{6.2}Al_{6.2}Si_{25.8}O_{64}$
Temperature/K	298
Space group	*Immm*
Radiation source	Neutrons
Diffractometer	Polaris
a/ Å **b/ Å** **c/ Å**	13.1589(11) 13.0652(10) 9.9754(8)
Volume/Å^3	1715.01(34)
R_p (bank 3)	0.0190
R_{wp} (bank 3)	0.0130
R_p (bank 4)	0.0187
R_{wp} (bank 4)	0.0140
R_p (bank 5)	0.0205
R_{wp} (bank 5)	0.0182
R_p (total)	0.0194
R_{wp} (total)	0.0143
χ^2	2.762

Table S17. Fractional atomic coordinates for $L_{6.2}$-MER

$Li_{6.2}$-MER	**x**	**y**	**z**	**Occup.**	**Multipl.**	**Uiso**
Si1	0.1121(4)	0.20926(28)	0.14831(30)	0.81	16	0.02809(13)
Al1	0.1121(4)	0.20926(28)	0.14831(30)	0.19	16	0.02809(13)
Si2	0.67539(27)	0.11046(28)	0.1549(4)	0.81	16	0.02809(13)
Al2	0.67539(27)	0.11046(28)	0.1549(4)	0.19	16	0.02809(13)
O1	0.19818(17)	0.12299(21)	0.18144(25)	1.0	16	0.02809(13)
O2	0.11589(31)	0.25118(23)	0.0	1.0	8	0.02809(13)
O3	0.0	0.14575(24)	0.1812(4)	1.0	8	0.02809(13)
O4	0.11777(22)	0.30869(20)	0.25480(30)	1.0	8	0.02809(13)
O5	0.65673(30)	0.14023(30)	0.0	1.0	8	0.02809(13)
O6	0.64458(26)	0.0	0.20830(33)	1.0	8	0.02809(13)
Li1	0.4188(13)	0.5	0.3026(13)	0.551(15)	8	0.01
Li2	0.5	0.1841(35)	0.395(4)	0.199(16)	8	0.01

2.3 Computer Simulation of Li cation positions in Li MER

Calculations for determining the potential Li sites in the framework were carried out using the 'Adsorption Locator' module from Materials Studio 2020. As with other calculations described in the paper, the COMPASS III forcefield was used and 'Fine' criteria were chosen for the energy calculations. A 2×2×2 all-silica narrow-pore MER supercell (a = 26.412 Å, b= 26.2826 Å, c = 19.9518 Å) with –48 charge spread over the whole framework was used as an input file. Simulated annealing calculations were set up to find the location of 48 Li cations within the supercell. This was meant to simulate a MER material with about 6 cations/unit cell. The simulation took place over 10 heating cycles with 5000 steps per cycle. The maximum temperature was set to 700 K and the final temperature was set to 300 K. The 10 lowest energy configurations were extracted as cif files and the positions of the Li cations compared with the most common cation sites found in MER structures so far. These sites are: Site I – D8R, Site II – between *pau* and *ste* cages (along the y direction), Site III – middle of the *ste* cage (along the z direction), Site III' – middle of *ste* cage (next to Site II) and Site IIIb – between *pau* and *ste* cages (next to Site III). A Python script was used to quantify the number of Li^+ cations in the above mentioned sites, considering the distance between the cation and the site as the criterion for their classification. The percentage of cations in each site is plotted below.

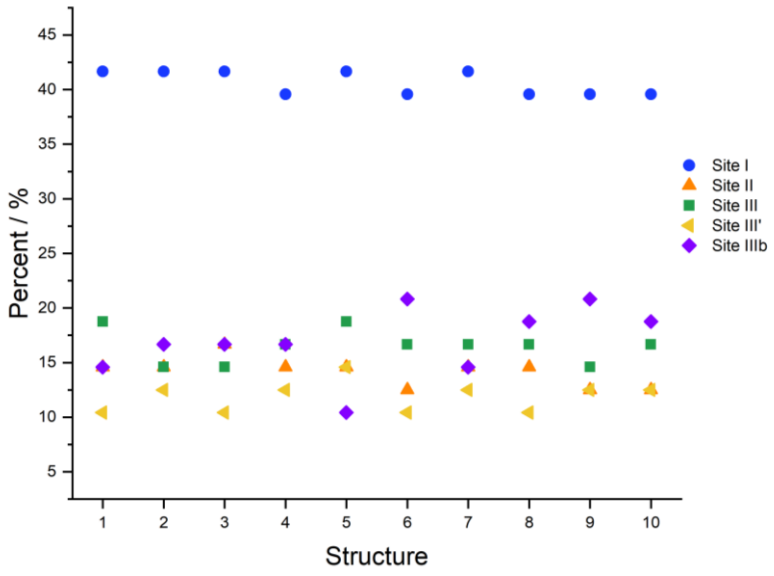

Figure S17. Li^+ cations' site occupation in the 10 lowest energy configurations found by the simulated annealing calculations, classified by their proximity to known cation sites in the MER structure.

These calculations reveal a strong affinity of the Li cations for site I in the narrow-pore MER structure. However, the uneven spread of 'occupancy' over the rest of the sites means that no definite conclusion can be drawn about the second most preferred site from this work.

2.4 VPXRD Fits

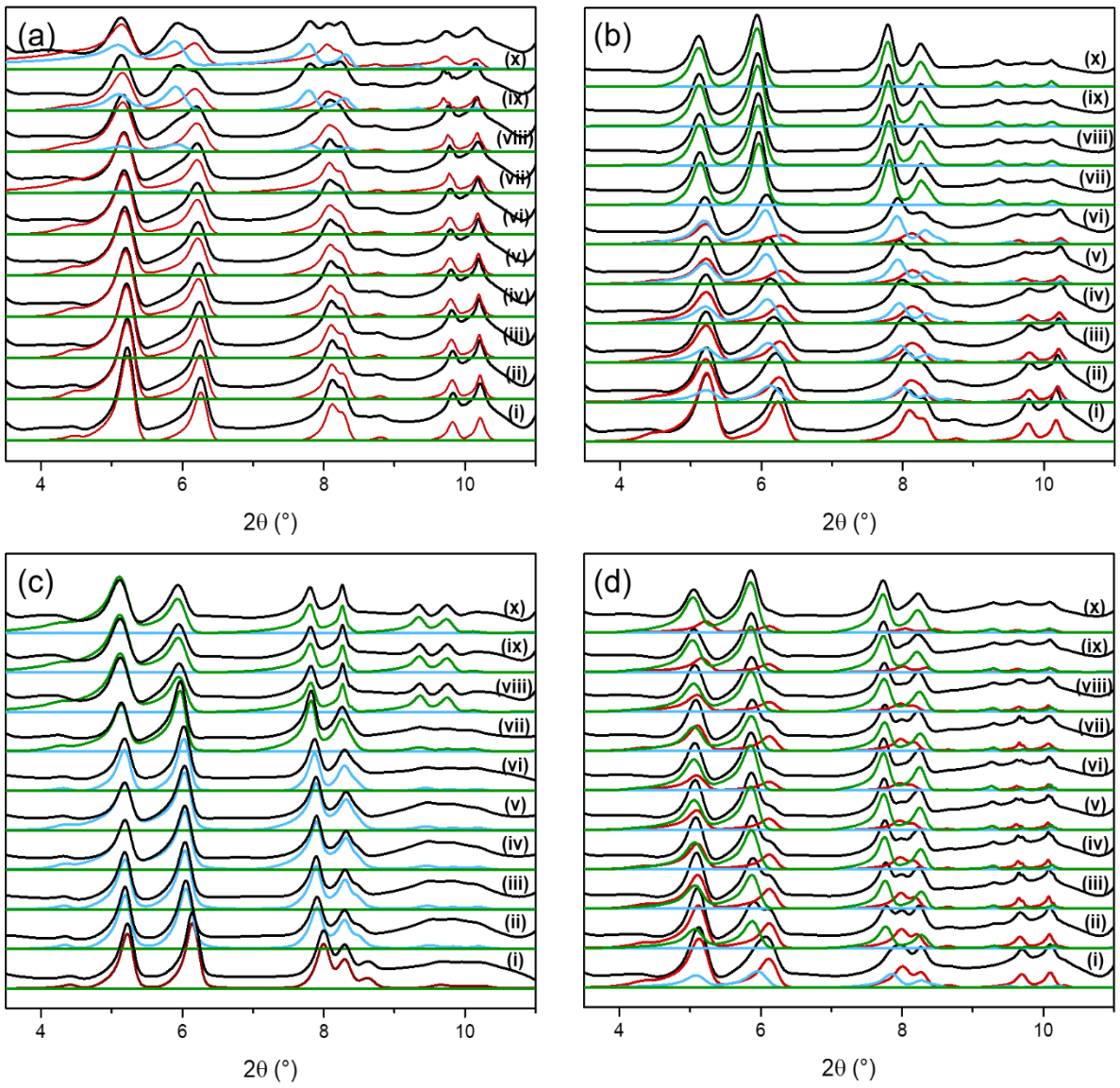

Figure S18. VPXRD calculated patterns of (a) $Li_{6.2}$-, (b) $Li_{4.0}Na_{2.2}$-, (c) $Li_{2.0}Na_{4.2}$- and (d) $Li_{4.0}K_{2.2}$-MER. Total, narrow-pore, intermediate and wide-pore phase patterns are shown in black, red, blue and green, respectively. Partial pressures of CO_2 during collection were (i) 20, (ii) 100, (iii) 200, (iv) 300, (v) 400, (vi) 500, (vii) 600, (viii) 700, (ix) 800 and (x) 1000 mbar.

2.5 Intermediate Structural Data

The following data was determined from $Li_{2.0}Na_{4.2}$-MER during a VPXRD experiment carried out at 500 mbar partial pressure of CO_2. Due to instrument limitations, VPXRD data is low quality and does not allow confident refinement. As such the following data possesses large uncertainty and should be deemed indicative of but not accurately describing the true crystal structure.

Table S18. $Li_{2.0}Na_{4.2}$-MER (ads – intermediate structure)

Site	Type	x	y	z	Occ.	Ω	B_{iso}
O1	O	0.20	0.16	0.17	1	16	1
O2	O	0.12	0.28	0	1	8	1
O5	O	0.67	0.11	0	1	8	1
O3	O	0	0.19	0.17	1	8	1
O6	O	0.69	0	0.22	1	8	1
O4	O	0.13	0.32	0.25	1	16	1
Si1	Si	0.11	0.23	0.14	0.81	16	1
Al1	Al	0.11	0.23	0.14	0.19	16	1
Si2	Si	0.69	0.10	0.18	0.81	16	1
Al2	Al	0.69	0.10	0.18	0.19	16	1
Na1	Na	0	0	0	0.13	2	2
Na2	Na	0.5	0.22	0	1	4	2
Na3	Na	0	0.5	0.5	0	2	2
C1	C	0.5	0.5	0	1	2	2
OC1	O	0.5	0.5	0.11	1	4	2

Table S19. Comparison of the narrow- and wide-pore $Li_{6.2}$-MER (dh) and (h) forms and intermediate form $Li_{2.0}Na_{4,2}$-MER window sizes.

Sample	I (Å)	IIa (Å)	IIb (Å)	III (Å)
$Li_{6.2}$-MER (dh)	1.4	1.3	3.0	1.1
$Li_{2.0}Na_{4.2}$-MER (ads - int)	2.6	1.9	3.5	2.7
$Li_{6.2}$-MER (h)	3.7	2.8	3.5	3.2

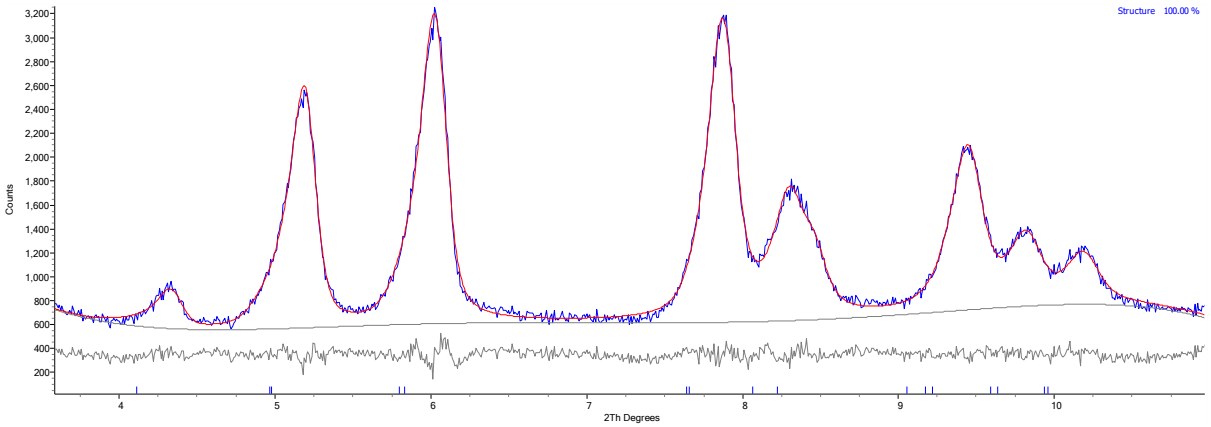

Figure S19. $Li_{2.0}Na_{4.2}$-MER (ads) Rietveld plot.

3. Carbon Dioxide Adsorption

3.1 High Pressure CO2 Adsorption on Li-MER

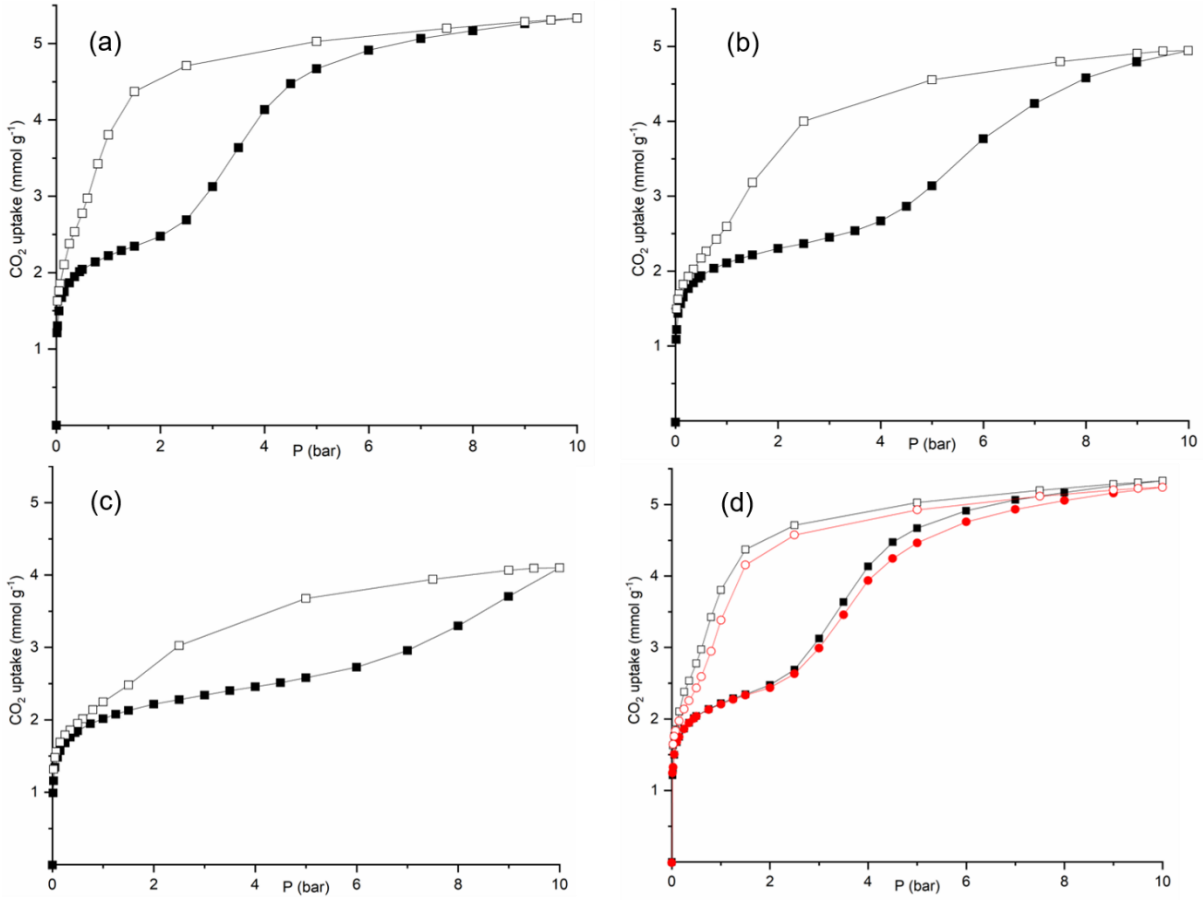

Figure S20. CO_2 sorption isotherms of $Li_{6.2}$-MER at (a) 298 K, (b) 313 K, (c) 328 K and (d) 298 K (comparison with a rerun, red) up to 10 bar. In each case the sample was degassed by heating under vacuum at 423 K between runs. Closed and open circles represent adsorption and desorption, respectively.

3.2 $Li_{6.2-x}M_x$-MER CO_2 Adsorption data

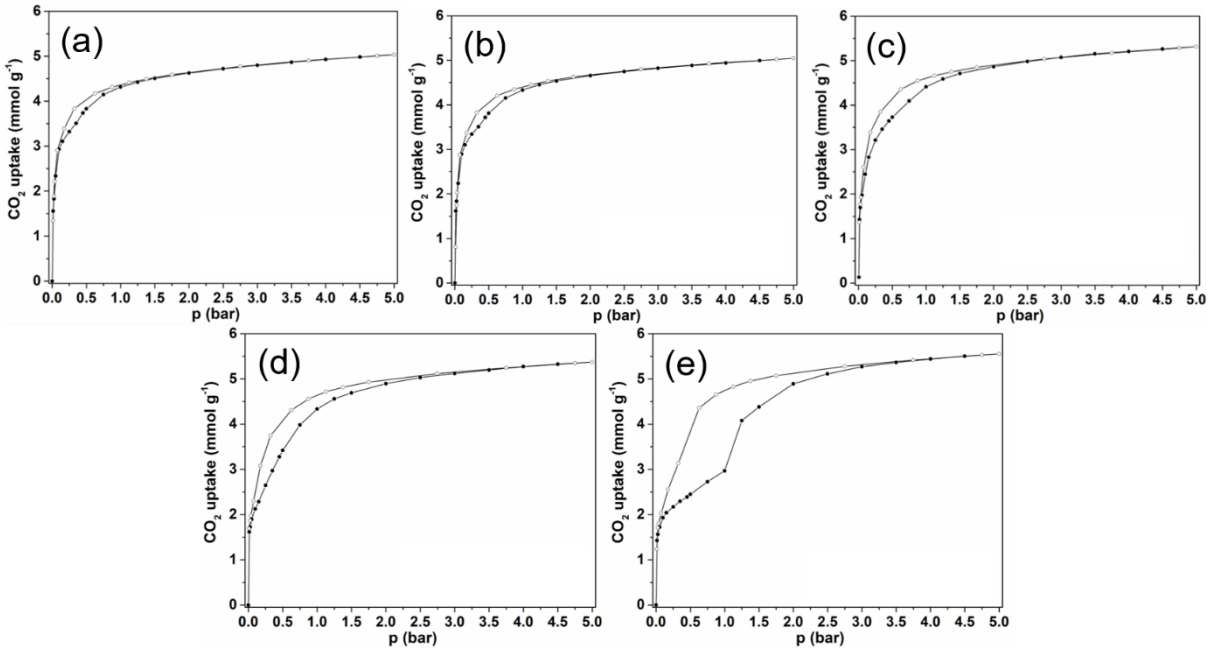

Figure S21. CO_2 sorption isotherms of the $Li_{6.2-x}Na_x$-MER series at 298 K up to 5 bar: (a) $Li_{1.0}Na_{5.2}$-, (b) $Li_{2.0}Na_{4.2}$-, (c) $Li_{3.0}Na_{3.2}$-, (d) $Li_{4.2}Na_{2.2}$- and (e) $Li_{5.0}Na_{1.2}$-MER. Closed and open circles represent adsorption and desorption, respectively.

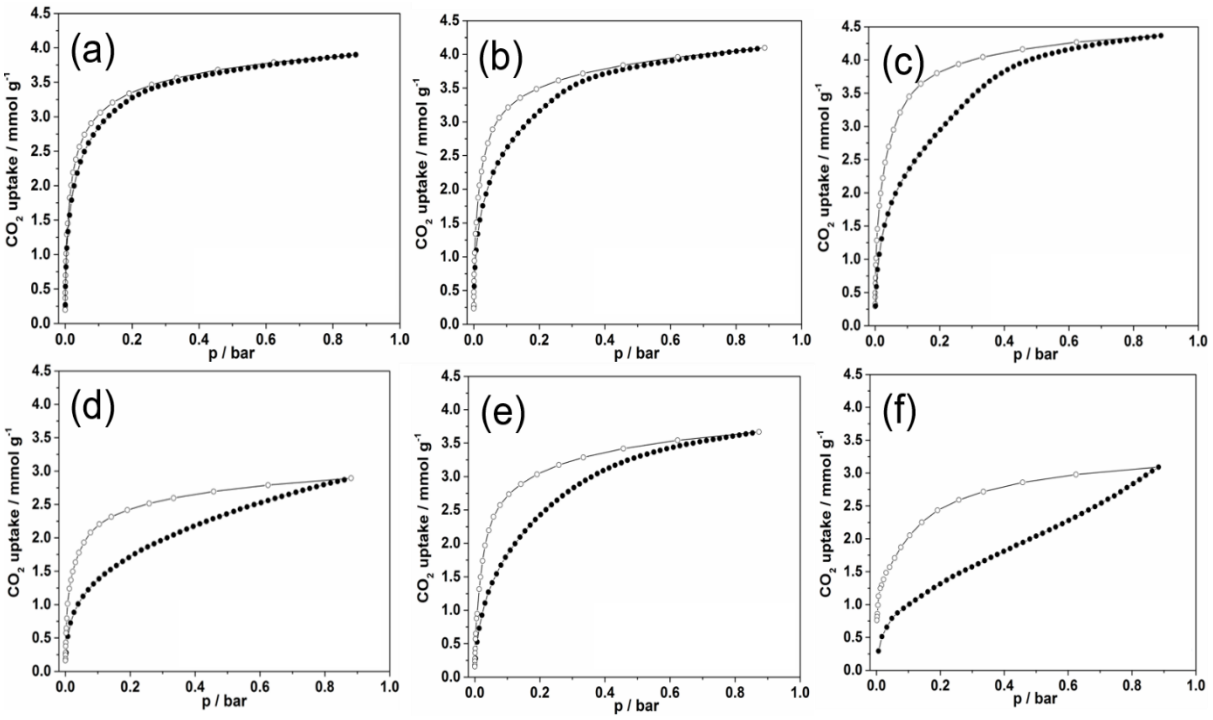

Figure S22. CO_2 sorption isotherms of the $Li_{6.2-x}K_x$-MER series at 298 K up to 1 bar: (a) $Li_{1.0}K_{5.2}$-, (b) $Li_{2.2}K_{4.0}$-, (c) $Li_{3.0}K_{3.2}$-, (d) $Li_{3.7}K_{2.5}$-, $Li_{4.0}K_{2.2}$- and (e) $Li_{5.0}K_{1.2}$-MER. Closed and open circles represent adsorption and desorption, respectively.

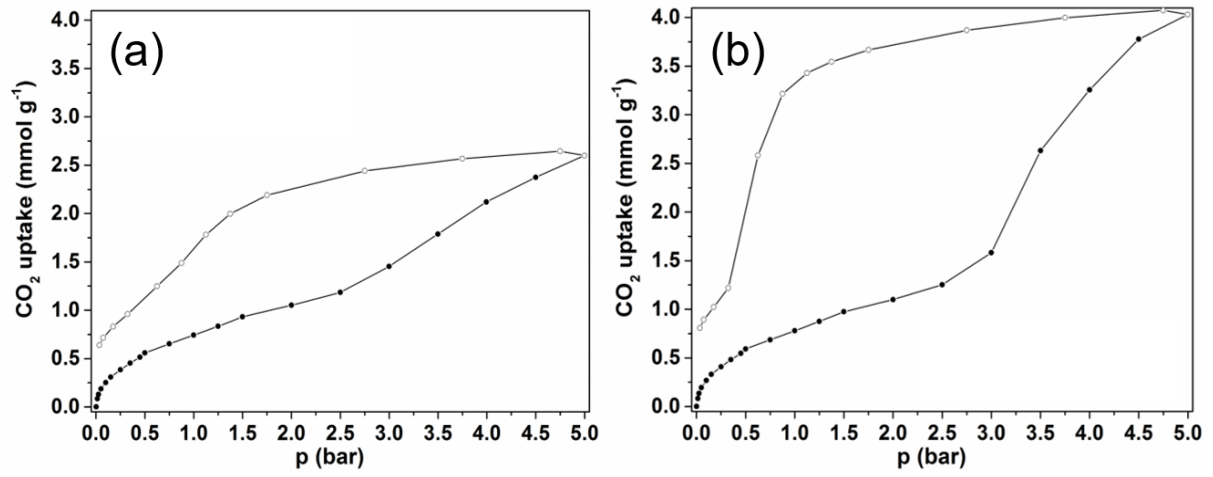

Figure S23. CO_2 sorption isotherms of the $Li_{6.2-x}Cs_x$-MER series at 298 K up to 5 bar: (a) $Li_{3.0}Cs_{3.2}$ and (b) $Li_{3.4}Cs_{2.8}$-MER. Closed and open circles represent adsorption and desorption, respectively.

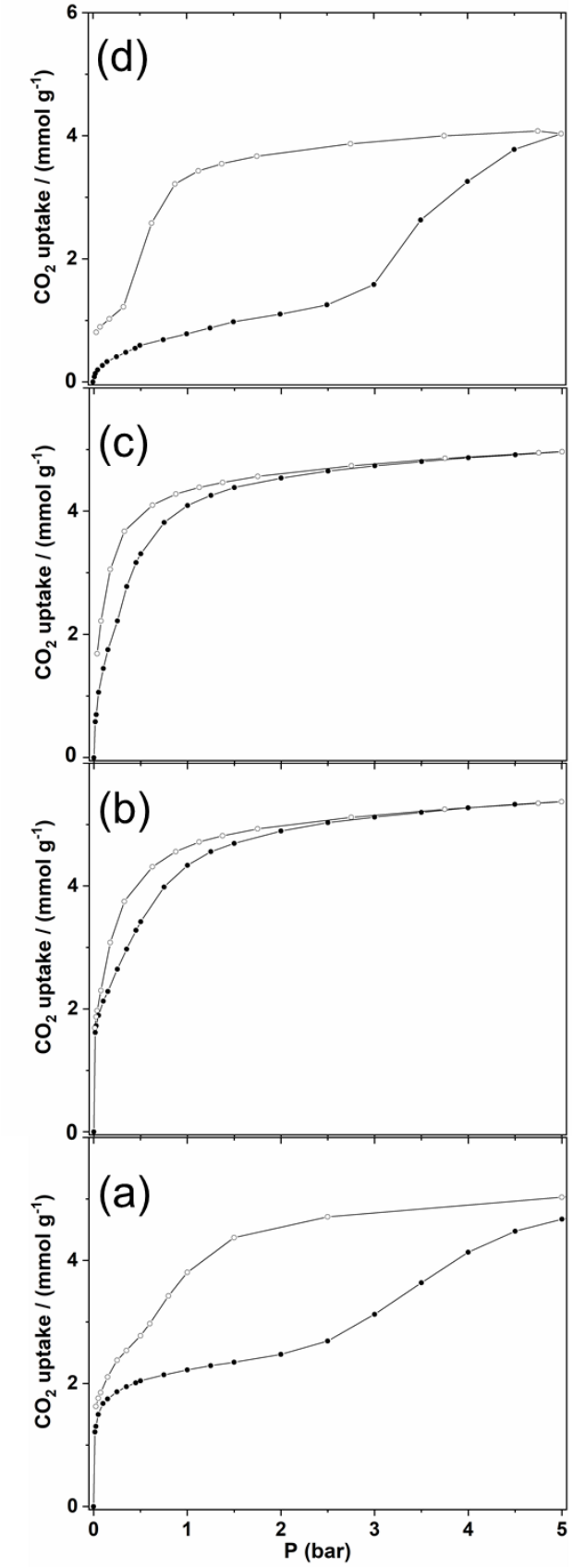

Figure S24. CO_2 adsorption isotherms at 298 K up to 5 bar for (a) $Li_{6.2}$-, (b) $Li_{4.0}Na_{2.2}$-, (c) $Li_{4.0}K_{2.2}$-, and (d) $Li_{3.4}Cs_{2.8}$-MER. Adsorption, closed symbols; desorption, open symbols.

4. Computational Simulation of CO_2 Adsorption

4.1 Simulated CO_2 Adsorption Isotherms of Li,Cs-MER

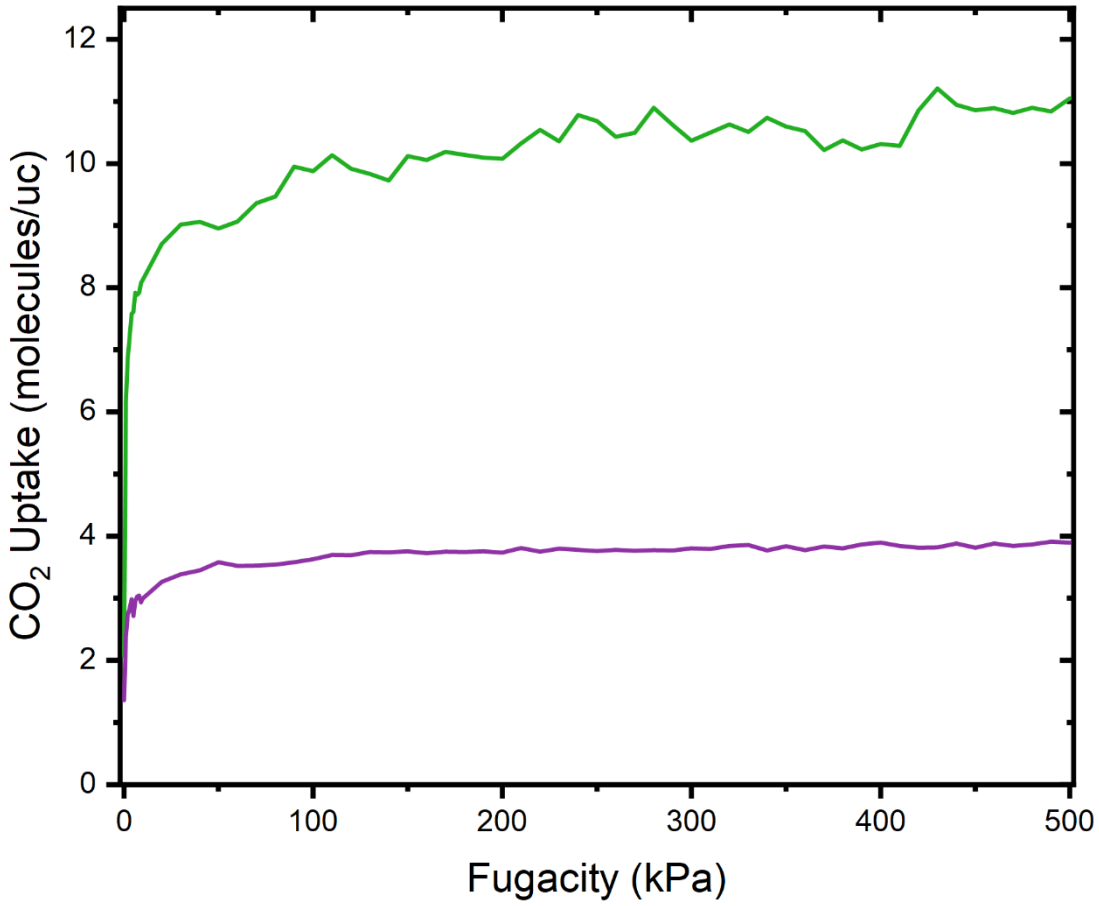

Figure S25. CO_2 adsorption 298 K isotherms simulated for Li,Cs-MER (with cations) in narrow pore (purple) and wide pore (green) forms.

4.2 Images of CO_2 Adsorption sites in Li-MER narrow and wide pore forms

To understand the potential siting of CO_2 within the MER materials, images were obtained from isotherm calculations for Li-MER framework in narrow and wide pore forms (no cations) described in the experimental method. They show a surface of constant density, coloured by the potential energy, probing the likelihood of CO_2 adsorption at a given site.

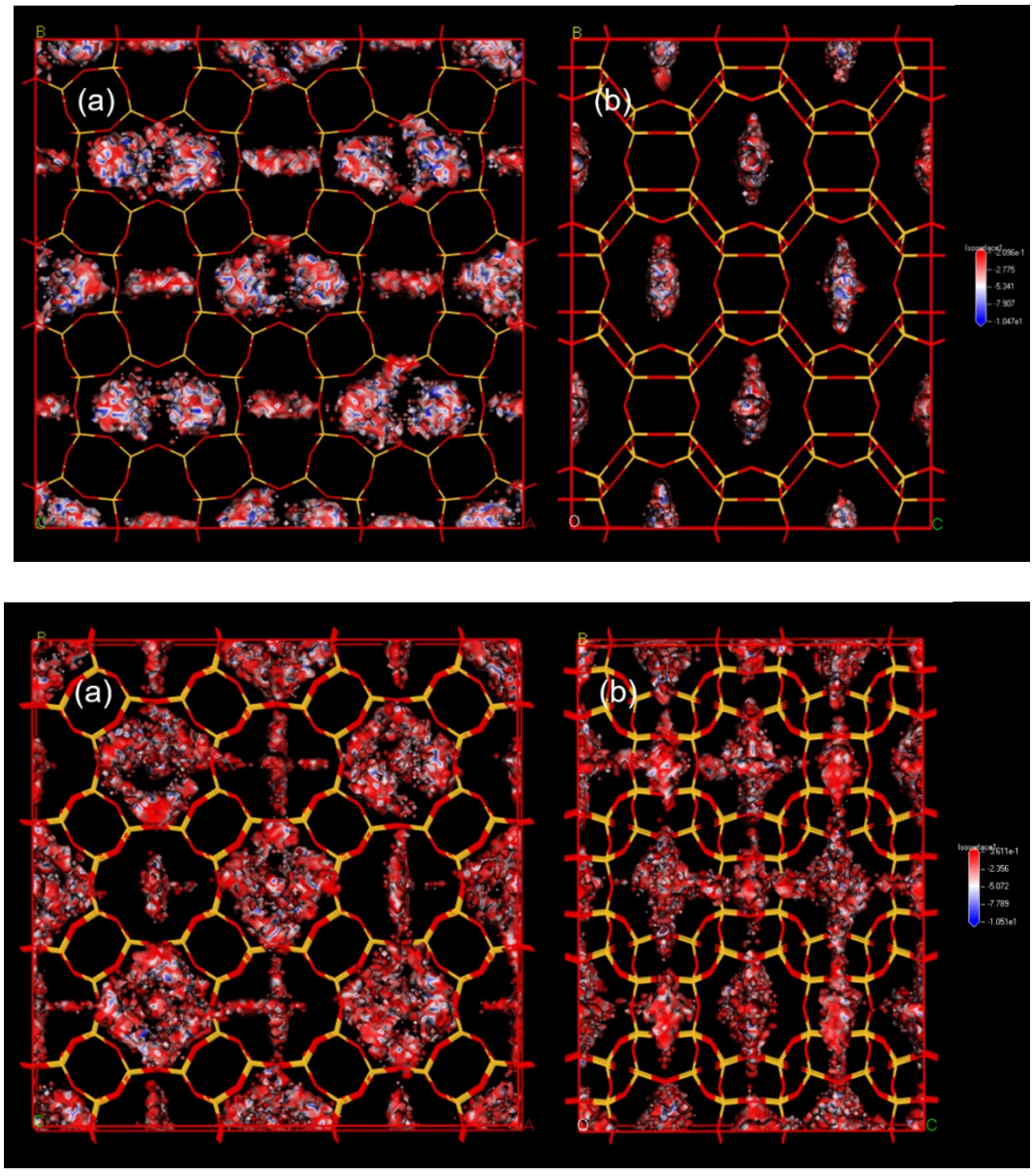

Figure S26. Potential energy distribution of CO_2 sites within (above) narrow-pore and (below) wide-pore silica MER, as viewed down the (a) z and (b) x axes. Red and blue correspond to least and most negative potential energies, as shown by the scale on the right.

5. TGA data

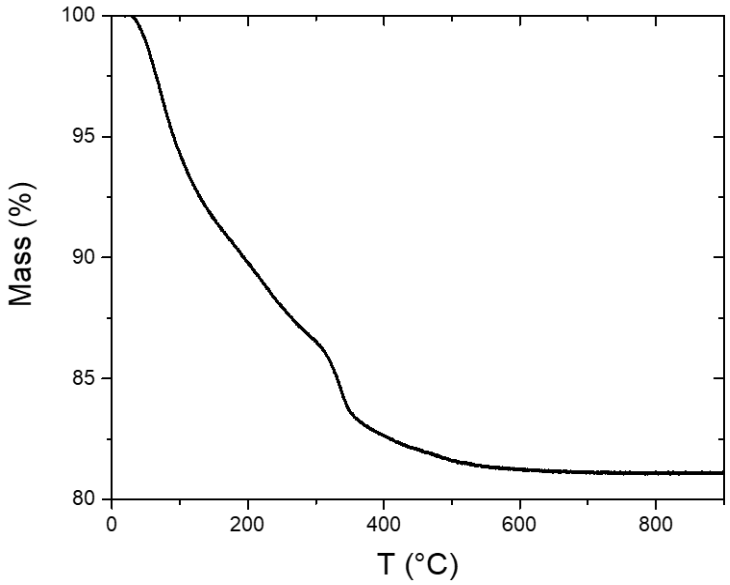

Figure S27. TGA data for $Li_{6.2}$-MER